Redox Mediation and Electron Transfer through Supramolecular Arrays of Ferrocene-Labeled Streptavidin on Biotinylated Gold Electrodes

Omar Azzaroni,*,†,‡ Marta Álvarez,† Mònica Mir,† Basit Yameen,† and Wolfgang Knoll†

Max-Planck-Institut für Polymerforschung, Ackermannweg 10, 55128 Mainz, Germany, and Instituto de Investigaciones Fisicoquímicas Teóricas y Aplicadas, CONICET, Universidad Nacional de La Plata, CC 16 Suc. 4 (1900), La Plata, Argentina

Received: June 04, 2008; Revised Manuscript Received: August 01, 2008

In this work we have studied electron transfer between ferrocyanide species in solution and Au electrodes redox-mediated by ferrocene labels linked to supramolecular bioconjugates. This configuration leads to the so-called electrochemical rectification where the ferrocyanide oxidation is mediated by electrogenerated ferricenium, as evidenced by a unidirectional current flux. Our aims were focused at gaining insight into the molecular aspects of the rectified current and exploring the limits of the electrocatalytic amplification when bioconjugates are used as a platform. We used the Alleman−Weber−Creager model to rationalize and describe in a more quantitative manner the influence of the donor species in solution on the measured electrocatalytic current. Moreover, this model enabled us to estimate homogeneous and heterogeneous rate constants associated with the electron transfer process. We observed that the characteristics of the redox-mediated amplification are highly dependent on the concentration of donor species. This can be described in two regimes depending on whether the bimolecular reaction (k_{cross}) or the electrogeneration of the mediator (k_o) is the limiting step in the overall electron transfer process. The estimation of k_{cross} is in good agreement with that calculated from Marcus theory. On the other hand, the k_o values suggest that electron transfer between the redox labels in the protein conjugate and the Au electrode is mainly controlled by electron tunneling through the biotinylated platform.

Introduction

Gaining a deeper understanding and designing novel strategies to manipulate electron transfer at the nanoscale is of mandatory importance in different research fields, for example, in chemistry, physics, and materials science. This is of interest for inherent scientific reasons but also because this knowledge constitutes the key to fully unravelling and controlling the mechanisms behind electron transfer processes in many technological applications.[1] Achieving nanoscale control over electron transfer properties of interfaces is a nontrivial task. In most cases, reaching this goal demands a multidisciplinary approach where the interplay between different fields such as chemistry, physics, biology, and materials science provides adequate tools to engineer this challenging subject.[2] A clear example is the integrated use of nanoparticle−biomolecule hybrid systems for wiring different nanostructures, like the DNA-templated carbon nanotube field-effect transistor,[3] or the controlled metallization of DNA strands to create Ag nanowires.[4] Other remarkable examples concern the tremendous advances in supramolecular electrochemistry[5] and photophysics[6] in order to create interfacial architectures with molecular-level accuracy and tailorable properties, to manipulate the photoinduced electron flow in a self-assembled supramolecular system[7] or to use rotaxane-based Langmuir−Blodgett films to the creation of electronically switchable tunnel junction devices.[8]

In dealing with nanoscale electron transfer, one of the primary interests is focused on so-called "molecular electronics".[9] That is the study of electronic processes measured and/or controlled on the scale of a single molecule. Moreover, in some cases this research field is called "unimolecular electronics" for emphasizing electron transfer processes involving not only single molecules but small clusters of molecules or molecules interrogated in parallel, as well.[10]

One of the simplest functions of a molecular device is current rectification or unidirectional current flow. This has been accomplished with different platforms such as self-assembled monolayers or Langmuir−Blodgett films.[11]

In particular, regarding current rectification at the solid−liquid interface, electrochemistry has attracted the interest of different researchers due to its straightforward and low-cost implementation combined with its simple readout. Pioneering works of Murray and co-workers[12] demonstrated that coating electrode surfaces with electroactive polymers was a versatile and convenient route for endowing them with new electronic properties.[13] This enabled the creation of rectifying electrochemical interfaces by using a clever strategy.

The approach consisted of modifying electrode surfaces with polymers containing redox centers. These redox sites were electrochemically oxidized and the charge was transported by "electron hopping" between the redox centers through the polymer inner environment.[14] Electron donors in solution in contact with the outermost polymer layer were oxidized by electron exchange with oxidized sites in the polymer. If the reverse reaction of electron acceptors in solution with reduced sites in the polymer was thermodynamically unfavorable or kinetically restricted and/or the transport of electron donors/acceptors to the electrode surface was hindered, then the current flowed in only one direction and the electrochemical interface acted as a current rectifier. This approach propelled the

* To whom correspondence should be addressed: e-mail azzaroni@mpip-mainz.mpg.de or azzaroni@inifta.unlp.edu.ar.
† Max-Planck-Institut für Polymerforschung.
‡ Universidad Nacional de La Plata.

10.1021/jp804938m CCC: $40.75
Published on Web 09/13/2008

widespread use of electroactive organic thin films to tailor the charge transfer properties of electrochemical interfaces.[15] It is worth noticing that these experimental findings were accompanied by rigorous theoretical work, which provided support and further extended the potentialities of the electrochemical rectification.[16] Later on, with the advent and progress of self-assembled monolayers, the approach was extended to the use of molecular films.[17] In this case, long-range electron transfer across monolayers was demonstrated to be the rate-limiting step.

This implies that the characteristics of the rectifying interface rely on a delicate balance between the electrochemical properties of the system, the electron transfer characteristics of the interacting species, and the nature of the interfacial architecture. Regarding this latter, self-assembly and supramolecular chemistry made fundamental contributions to achieve molecular-level control of the chemical topology and dimensions of nanoscale architectures at interfaces.[18] This has been of fundamental importance if we consider how sensitive the interfacial electron transfer is to structural details such as surface coordination or the chemical identity of building blocks.[19]

Along these lines, we used redox-labeled supramolecular bioconjugates as molecular modules to create rectifying interfaces promoting unidirectional flow. In this work, we devote special attention to the study of physicochemical and molecular aspects of the rectified current. We also explore the origin of the limits on redox-mediated current amplification as well as the rate-determining steps of electron transfer. These are all relevant issues considering the rather unexplored nature of current rectification and electron transfer through nanoassemblies held together by supramolecular forces of biological origin. We are confident that these results will promote a deeper understanding of electron transfer processes occurring in nanoconfined environments and provide a new approach to the molecular design and manipulation of electron transport properties at biointerfaces.

Experimental Section

Materials. Potassium ferrocyanide, phosphate-buffered saline (PBS), *N*-hydroxysuccinimide (NHS), dimethylformamide (DMF), [*N*-(3-dimethylaminopropyl)-*N*′-ethylcarbodiimide hydrochloride] (EDC), and 11-mercaptoundecanol were purchased from Sigma−Aldrich. Streptavidin from *Streptomyces avidinii* was supplied by Serva (Germany). Biotin-terminated thiol [**1**, 12-mercaptododecanoic (8-biotinoylamido-3,6-dioxaoctyl)amide] was obtained from Boehringer Mannheim. [*N*-(Ferrocenylmethyl)-6-amino)hexanoic acid was synthesized as previously described by Shoham et al.[20]

Synthesis of Ferrocene-Labeled Streptavidin. The redox-labeled protein was synthesized at the Max-Planck-Institut für Polymerforschung following procedures reported in the literature.[21] Briefly, [*N*-(ferrocenylmethyl)-6-amino)hexanoic acid (36 mg), *N*-hydroxysuccinimide (14 mg), and [*N*-(3-dimethylaminopropyl)-*N*′-ethyl-carbodiimide hydrochloride] (22 mg) in 1 mL of dry DMF were heated under N_2 atmosphere with stirring at 80 °C for 1.5 h. Nine aliquots (10−15 μL) of this solution were added to a solution of 2 mg of streptavidin in 1 mL of PBS buffer (0.1 M, pH 7.4). The solution was stirred overnight at room temperature with the appearance of some precipitates. The precipitates were removed by centrifugation and the supernatant was dialyzed against 0.1 M PBS buffer (pH 7.4) to remove the unreacted ferrocene. The spectrophotometrically determined Fc/SAv ratio was ∼4. The biotin binding capacity of Fc-SAv was found to be similar to that of SAv (see below).

Electrochemical Measurements. Cyclic voltammetry experiments were performed with an Autolab potentiostat using a conventional three-electrode cell equipped with an Ag/AgCl reference electrode and a graphite counterelectrode.

Surface Plasmon Resonance. SPR detection was carried out in a homemade device using the Kretschmann configuration.[22] The SPR substrates were BK7 glass slides evaporation-coated with 2 nm of chromium and 50 nm of gold. The substrates were incubated overnight with a mixture (1:9) of biotin-terminated thiol and 11-mercapto-1-undecanol. Then the surface was carefully rinsed with ethanol and dried with N_2, followed by 2 h of incubation in 1 μM Fc-SAv + 0.1 M PBS buffer. The same buffer was used to rinse the biomolecules that were not specifically bound to the biotinylated surface. Before and after injection of the Fc-SAv solution in the liquid cell, the SPR signal at different angles was recorded. This was done to detect the shift of the minimum angle of reflectance due to protein bioconjugation on the surface. The SPR angle shifts were converted into mass uptakes via the experimentally determined relationship, Γ (nanograms per square millimeter) = $\Delta\theta$ (degrees)/0.19. The sensitivity factor was obtained by procedures reported in the literature.[23]

SPR was also used to estimate the equivalent thickness of the biotinylated platform. The procedure has been described in detail elsewhere.[22] The equivalent thickness of the biotinylated SAM was calculated from the SPR optical thickness (*nd*) measured before and after formation of the self-assembled monolayer, where a refractive index of $n = 1.42$ for the layer was assumed.

Atomic Force Microscopy. Images were taken in air at room temperature with a commercial AFM Dimension 3000 (Veeco) controlled with a Nanoscope V, operating in the tapping mode. Silicon cantilevers (Olympus) 160 μm long, 50 μm wide and 4.6 μm thick, with an integrated tip of a nominal spring constant of 42 N/m and a resonance frequency of 300 kHz, were used. In a typical experiment, the tip was scanned at velocities in the range of 0.8−1 Hz and minimal applied forces were used when imaging. Topography and phase images were used to record the structures. Samples for AFM analysis were prepared by immersing overnight freshly prepared gold-coated ultraflat mica surfaces in the mixed thiol solution. After careful rinsing with ethanol, the biotinylated substrates were incubated for 2 h with a 1 μM Fc-SAv in 0.1 M PBS buffer. The samples were then rinsed with water, dried with nitrogen, and shielded from dust particles.

Results and Discussion

Building Up the Supramolecular Interfacial Architecture. In order to construct the rectifying interfacial architecture, we initially chemisorbed on the Au electrode a self-assembled monolayer (SAM) containing the biotin ligand. This platform was constructed as a binary SAM containing a biotin-terminated thiol [12-mercaptododecanoic (8-biotinoylamido-3,6-dioxaoctyl)amide, **1**] and a hydroxy-terminated thiol (11-mercaptoundecanol) in a 1:9 ratio. This particular composition provides the optimum coverage of biotin centers for obtaining maximum streptavidin (SAv) binding.[24]

Then, ferrocene-labeled SAv (Fc-SAV) containing 4 ferrocene centers per protein was bound to the biotinylated electrode surface (Figure 1). The affinity of SAv for biotinylated compounds is extremely high ($K = 10^{15}$ L mol^{-1}) involving very specific interactions and leading to a very stable linkage.[25]

To characterize the Fc-SAv bioconjugation, we followed the immobilization by surface plasmon resonance (SPR). As

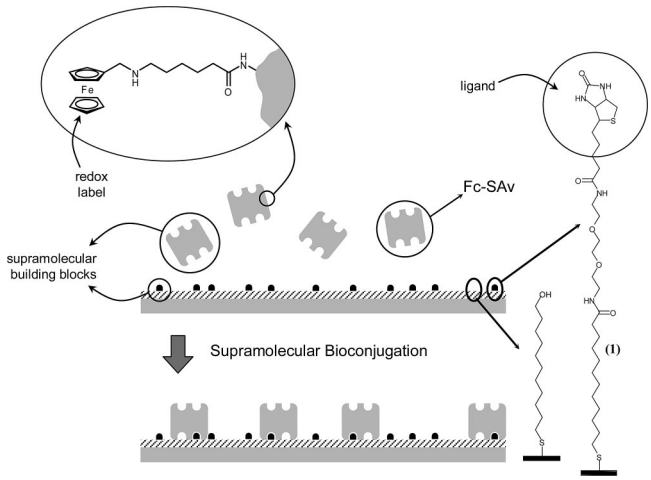

Figure 1. Simplified cartoon describing the supramolecular bioconjugation of Fc-SAv onto the biotinylated electrode. Also shown are the chemical structures of the ferrocene linker and the functionalized thiols constituting the biotinylated platform.

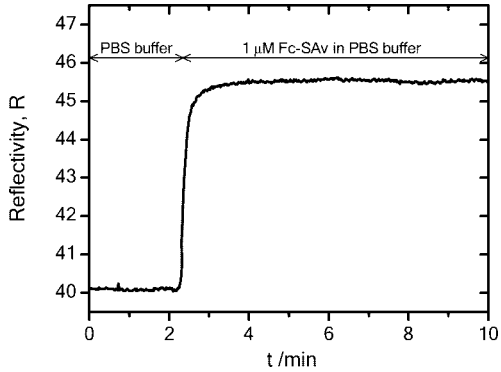

Figure 2. SPR sensorgram corresponding to bioconjugation of Fc-SAv onto the biotinylated Au electrode.

depicted in Figure 2, the SPR measurements indicated that the conjugation on the biotinylated Au surface is very fast and within a few seconds the protein coverage reaches a well-defined plateau.[26]

An estimate of the mass of protein conjugated on the electrode was derived from the shift in the minimum of the angular θ-scans of reflected intensity (Figure 3). This $\Delta\theta$ is related to a mass uptake that corresponds to a coverage of 226 ng/cm^2, which is equivalent to 2.2×10^{12} Fc-SAv molecules/cm^2.

This value is in excellent agreement with X-ray photoelectron spectroscopy and near-edge X-ray absorption fine structure measurements on similar biotinylated SAMs reported by Nelson et al.,[27] who estimated 230 ng$\cdot$cm^{-2} for the SAv coverage. These results indicate that labeling of the protein does not affect its biotin-recognition properties.

In our sample preparations, bioconjugation was accomplished by placing the biotinylated electrode in a 1 μM Fc-SAv solution (in PBS) for 2 h. This led to the creation of a self-assembled interface with the redox centers lying on the protein layer.

Careful examination with atomic force microscopy (AFM) revealed a homogeneous distribution of the protein on the electrode surface (Figure 4). This is represented by the random array of globular objects 2−2.5 nm in average height and 15−20 nm in diameter (as measured at midheight). The bright nodular objects in the AFM image indicate the distribution of single and small groups of Fc-SAv molecules on the biotinylated surface. This picture is in full agreement

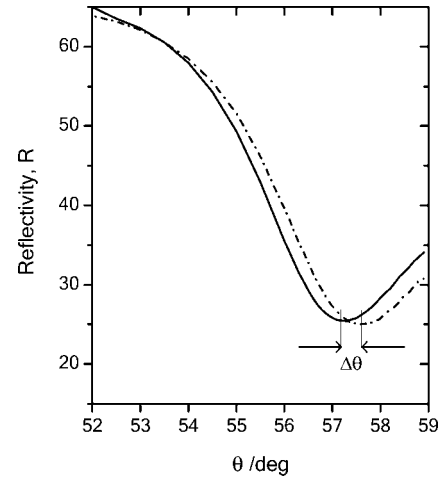

Figure 3. Reflectivity curves as a function of the angle-of-incidence scan (θ). The plot describes the changes occurring in a biotinylated Au electrode (—) before and (---) after incubation in 1 μM Fc-SAv (in 0.1 M PBS buffer). $\Delta\theta$ is proportional to the mass of protein bioconjugated on the electrode surface.

with recent results reported by Ihalainen and Peltonen[28] describing the immobilization of nonlabeled SAv on biotinylated lipid bilayers.

Even if it is well-known that tip−sample convolution always introduces distortions on the lateral dimensions of the measured objects,[29−31] AFM imaging clearly shows that the protein is randomly and homogeneously distributed on the Au surface.

Electroactivity and Redox-Mediated Electron Transfer. As previously described, the rectifying interface is constructed from three building parts: the Au electrode, the biotinylated SAM, and the ferrocene-labeled protein. Considering that electron transfer takes place across the entire interface, we characterized each part of the interfacial architecture separately before proceeding to redox mediation experiments.

Figure 5a describes the cyclic voltammetry of a bare Au electrode in the presence of $Fe(CN)_6^{4-}$ species. The voltammetric response shows a reversible electrochemical response, indicating the feasibility of electron transfer between the redox species in solution and the metal electrode. Chemisorbing the biotinylated SAM on the Au electrode generates a metal surface that is completely blocking (Figure 5b). This experimental observation is due to the fact that the biotinylated platform is constituted of long-chain alkanethiols that preclude direct electron transfer between the $Fe(CN)_6^{4-}$ species and the Au electrode.[32] This is in complete agreement with earlier work of Finklea et al.[33] demonstrating the blocking characteristics of long-chain SAMs.

Cyclic voltammograms of Fc-SAv bionjugated onto the biotinylated electrode demonstrate that electron transfer across the supramolecular bioconjugate is achievable and consequently the redox labels are "wired" to the electrode. The charge associated with the oxidation/reduction process of these ferrocene labels (as estimated from the voltammetric response) is 1.3 ± 0.2 μC/cm^2, that is, 8×10^{12} ferrocene centers/cm^2. On average each SAv molecule carries four Fc labels, so the electrochemical measurement reflects a protein surface density of $\sim 2 \times 10^{12}$ molecules/cm^2. This value is in very good agreement with that previously estimated by SPR measurements.

Next, we proceed to redox-mediated electrocatalysis. By controlling the electrode potential, we can easily oxidize or reduce the ferrocene moieties in the bioconjugates. The presence of electron donors in solution interacting with electron acceptors

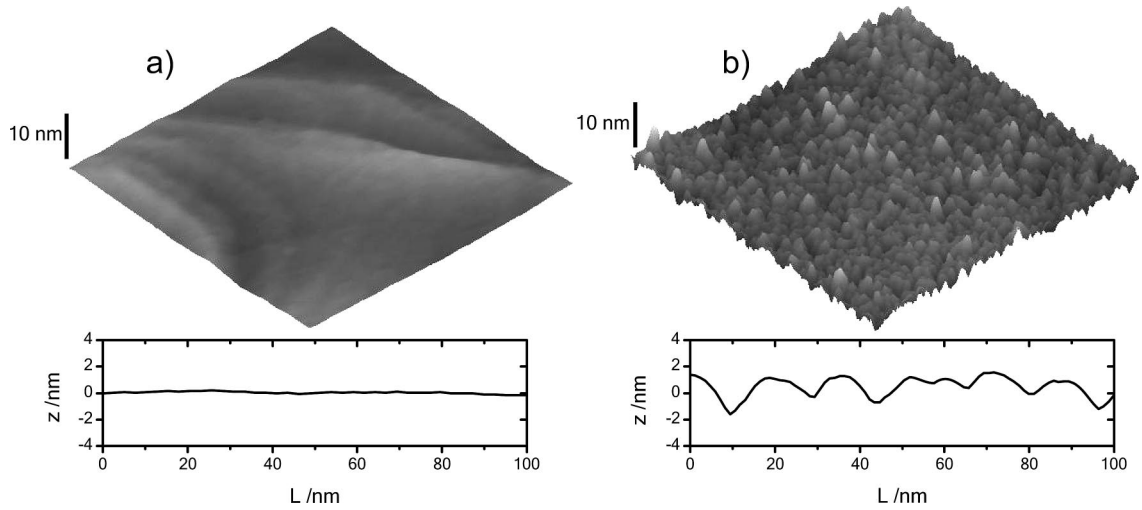

Figure 4. (a) Three-dimensional atomic force microscopic images (500 × 500 nm^2) showing (a) a biotinylated Au electrode and (b) the same electrode after bioconjugation with 1 μM Fc-SAv in 0.1 M PBS buffer. Corresponding cross-sectional analyses are also included.

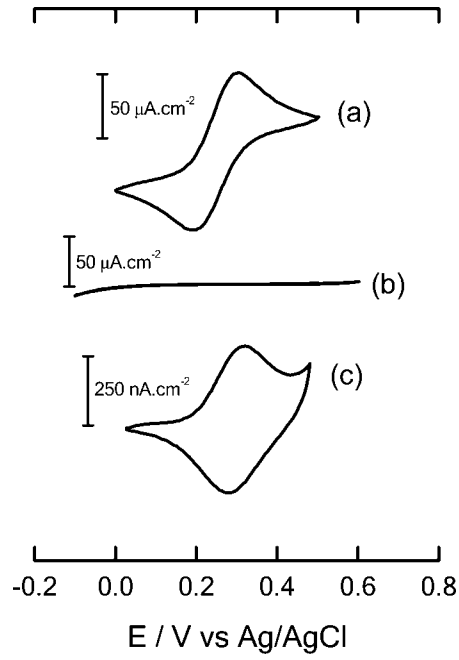

Figure 5. Cyclic voltammograms corresponding to (a) bare and (b) biotinylated Au electrode in the presence of 1 mM $Fe(CN)_6^{4-}$ in 0.1 M PBS buffer. (c) Fc-SAv bioconjugated on a biotinylated Au electrode in 0.1 M PBS buffer (pH = 7.4). In all cases the scan rate, υ, was 50 mV/s.

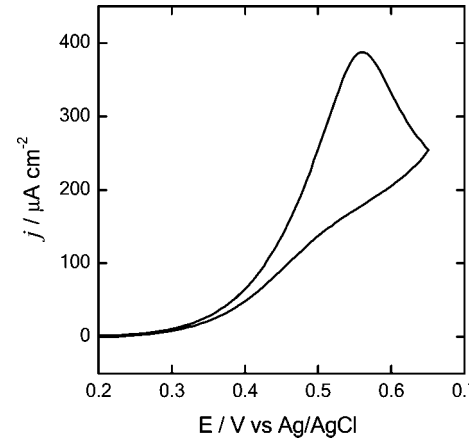

Figure 6. Cyclic voltammogram representing the electrochemical response of a Fc-SAv-modified Au electrode in the presence of 5 mM $Fe(CN)_6^{4-}$ in 0.1 PBS buffer. υ = 20 mV/s, T = 298 K.

in the protein layer could lead to electron exchange with the supramolecular bioconjugate. These charge transfer processes should be evidenced as an anodic current.[17] On the other hand, if interaction between electron acceptors in solution and electron donors in the bioconjugate is thermodynamically restricted, electron transfer will not be initiated and, consequently, no cathodic current will be sensed.

This is the basis of electrochemical rectification, and with adequate choice of donors and acceptors, this can be easily achieved experimentally.[34] Figure 6 shows the voltammetric response of a FcSAv-modified Au electrode in the presence of ferrocyanide. Electrochemical rectification is evidenced as a notorious anodic peak, while no cathodic peak is observed. The anodic current peak originates from ferrocyanide oxidation mediated by the ferrocene/ferricenium species in the bioconjugated layer. The absence of a cathodic signal after reversal of the potential scan is attributed to the fact that the electrogenerated ferrocene is not strong enough to reduce the ferricyanide, hence there is no electron exchange.

Interpretation of Redox-Mediated Electron Transfer Based on the Alleman−Weber−Creager Approach. Having shown that current rectification occurs through electron transfer mediated by redox labels in the supramolecular bioconjugate, we proceed to estimation and analysis of the relevant factors responsible for this redox mediation. This will provide information at the molecular level about the key factors governing nanoconfined electron transfer in the protein−electrode environment. Proceeding to the analysis requires a physical model that could describe the observed phenomenon in a more quantitative manner. In our case, we will describe electrochemical rectification using the formalism developed by Alleman, Weber, and Creager, which we will refer to as the AWC approach.[17] For the sake of clarity and as a background for the discussion, we will briefly revisit the general ideas of this approach in this section.

This physical model is very simple, describing the electrochemical oxidation of an electron donor D in solution by a surface-immobilized redox center that acts as a mediator, R/O:

$$\mathrm{R} \underset{k_{\mathrm{red}}}{\overset{k_{\mathrm{ox}}}{\rightleftharpoons}} \mathrm{O} + ne$$

$$^{-}\mathrm{O} + \mathrm{donor} \xrightarrow{k_{\mathrm{cross}}} \mathrm{R} + \mathrm{acceptor}$$

This physical picture describes the interplay between three critical parameters influencing the electron transfer: the homogeneous rate constant for the reaction of the oxidized redox labels with electron donors in solution (k_{cross}, in M^{-1} s^{-1} units) and the heterogeneous rate constants for reduction (k_{red}, in s^{-1} units) and oxidation (k_{ox}, in s^{-1} units) of the surface-confined redox centers.

It is worth noting that, in spite of its very elementary character, the model has been successfully applied to the description of electrochemical rectification via self-assembled monolayers. In that case, it has been demonstrated that the kinetic parameters estimated by the AWC approach are in good agreement with those estimated by other electrochemical techniques.[17] This is clear evidence that this physical model can be used as a very simple yet useful and powerful tool for estimating electron transfer-related parameters derived from redox mediation experiments.

In the AWC approach, the overall reaction rate is considered to be the rate of acceptor production through the reaction of donor species in solution with the oxidized surface-confined mediator:

$$\frac{j}{nF} = k_{\mathrm{cross}} c_{\mathrm{D}} \Gamma_{\mathrm{ox}} \tag{1}$$

where j is the current density, n is the number of electrons involved in the reaction, F is the Faraday constant, c_{D} is the concentration of electron donor species in solution, and Γ_{ox} is the concentration of oxidized mediator at the electrode surface.

Furthermore, the model makes use of the steady-state assumption for the oxidized mediator, such that the surface concentration of oxidized mediator does not change with time:

$$\frac{\partial \Gamma_{\mathrm{ox}}}{\partial t} = (k_{\mathrm{ox}} \Gamma_{\mathrm{red}}) - (k_{\mathrm{red}} \Gamma_{\mathrm{ox}}) - (k_{\mathrm{cross}} \Gamma_{\mathrm{ox}} c_{\mathrm{D}}) = 0 \tag{2}$$

In accordance with the steady-state assumption, Γ_{ox} is given by

$$\Gamma_{\mathrm{ox}} = \frac{k_{\mathrm{ox}} \Gamma_{\mathrm{red}}}{k_{\mathrm{red}} + (k_{\mathrm{cross}} c_{\mathrm{D}})} \tag{3}$$

At this point the physical model described by Creager and coworkers introduces the simplifying assumption that $\Gamma_{\mathrm{ox}} \ll \Gamma_{\mathrm{red}}$, thus leading to $\Gamma_{\mathrm{T}} \sim \Gamma_{\mathrm{red}}$. As a consequence, the final expression describing the electrochemical current is

$$\frac{j}{nF\Gamma_{\mathrm{T}}} = \frac{k_{\mathrm{ox}} k_{\mathrm{cross}} c_{\mathrm{D}}}{k_{\mathrm{red}} + (k_{\mathrm{cross}} c_{\mathrm{D}})} \tag{4}$$

The AWC model mostly relies on two essential assumptions: (a) the concentration of donor species at the electrochemical interface is not significantly perturbed by the mediation reaction (concentration polarization), and (b) during the course of mediated electron transfer, the concentration of the mediator in the reduced state is larger than that corresponding to the oxidized state ($\Gamma_{\mathrm{red}} \gg \Gamma_{\mathrm{ox}}$).

As noted and demonstrated by the authors who proposed the model, these two conditions can be experimentally fulfilled when working on potential regions near the foot of the voltammetric wave. In that case, conversion of the mediator from the reduced to the oxidized form is rather low and the system is, in principle, far from the diffusion-limited regime, thus avoiding concentration polarization. This fact indicates that all quantitative analysis with the AWC model should be restricted to these particular experimental conditions in order to obtain reliable information.

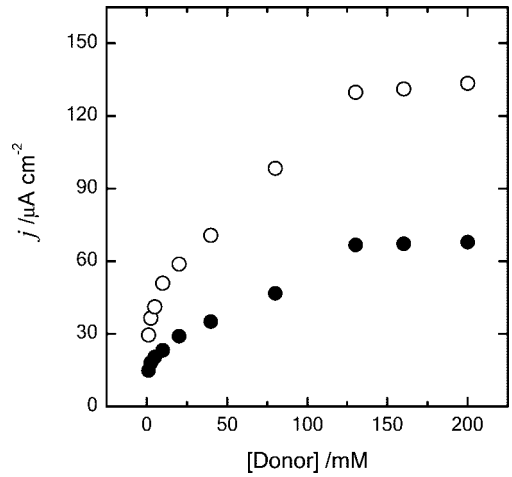

Figure 7. Plots describing the variation of electrocatalytic current measured at (•) 0.33 V and (○) 0.37 V vs Ag/AgCl as a function of the donor $[Fe(CN)_6^{4-}]$ concentration, c_{D}.

The mathematical expression indicated in eq 4 has two limiting cases corresponding to two kinetic regimes. One case is the situation where $k_{\mathrm{red}} \gg k_{\mathrm{cross}} c_{\mathrm{D}}$, thus implying that the bimolecular reaction between the oxidized mediator (electron acceptor) and the electron donor is the limiting factor in the overall rate. The other one is $k_{\mathrm{red}} \ll k_{\mathrm{cross}} c_{\mathrm{D}}$, with the consequence that electrochemical generation of the mediator is limiting the reaction rate.

For these two limiting cases, eq 4 can be rewritten as

$$\text{case I} \qquad \frac{j}{nF\Gamma_{\mathrm{T}}} = k_{\mathrm{cross}} c_{\mathrm{D}} \frac{k_{\mathrm{ox}}}{k_{\mathrm{red}}} \tag{5}$$

$$\text{case II} \qquad \frac{j}{nF\Gamma_{\mathrm{T}}} = k_{\mathrm{ox}} \tag{6}$$

It can be clearly seen that one regime (case I) is dependent on the donor concentration, while the other one (case II) is independent. This is a relevant and important aspect of the AWC approach because it explicitly describes and provides an expression for the situation where generation of the mediator is the limiting step. As a consequence, the rectified current measured at a given potential should reach a plateau upon increasing the donor concentration.[17] Experimentally this should be done by estimating the current density for different c_{D} values at exactly the same potential, due to the fact that k_{red} and k_{ox} are potential-dependent variables.

In the case of ferrocene-labeled supramolecular bioconjugates, the redox-mediated current clearly shows a plateau as predicted by the AWC model. Figure 7 shows the variation of redox-mediated electrocatalytic current with c_{D} measured at two different potentials. Due to the fact that k_{red} and k_{ox} are potential-dependent variables, an increase of the potential is reflected as a higher electrocatalytic current. However, it is evident that for both potential conditions the trend is exactly the same. We can infer that for $Fe(CN)_6^{4-} < 100-120$ mM we are in a c_{D}-dependent regime (i.e., case I), while for $Fe(CN)_6^{4-} > 100-120$ mM we entered into the plateau, which is characteristic of case II. This experimental observation supports the idea

of a molecular-level scenario where different mechanisms are dominant under different c_D conditions.

Referring to the expressions describing the two limiting cases, we have to consider that k_{ox} and k_{red} are two potential-dependent parameters that, within certain limits,[35] can be described with the Butler−Volmer equation.[36] This leads to the following simple equations for the current density as a function of the applied potential:

$$\text{case I} \qquad \frac{j}{q} = k_{cross} c_D \exp\left[\frac{nF}{RT}(E - E^\circ)\right] \tag{7}$$

$$\text{case II} \qquad \frac{j}{q} = k_0 \exp\left[\frac{(1-\alpha)nF}{RT}(E - E^\circ)\right] \tag{8}$$

In both expressions the term $nF\Gamma_T$ has been replaced by q, the charge density associated with oxidation/reduction of the surface-confined redox centers (mediators). Particularly in case II, by introducing the formalism of Butler−Volmer we are now describing the electron transfer process in terms of the transfer coefficient (α) and the standard electron transfer rate constant (k_o). These expressions indicate that we can obtain the relevant parameters describing the electron transfer process by simply analyzing the dependence of j on E in both kinetic regimes.

Estimation of Rate Constant for the Bimolecular Electron Transfer Reaction, k_{cross}. One of the important parameters describing the rectified electrochemical current is the rate constant of electron transfer between electron donors in solution and surface-confined redox mediators. As we can see in eq 7, a semilogarithmic j/q versus potential representation should describe a slope equivalent to 38.96 V^{-1} and would provide the value of k_{cross} from the intercept at $E°$. Figure 8 depicts the current−potential plot derived from the experimental values obtained when working at a very low electron donor concentration [120 μM $Fe(CN)_6^{4-}$ in 0.1 M PBS] (i.e., in the case I regime).

The slope of the straight line is 38.7 ± 0.1 V^{-1}, which is in excellent agreement with the expected value from the AWC model (38.9 V^{-1}). This value reinforces the idea that, at very low donor concentrations, the main factors governing the generation of electrochemical rectified current can be described by case I, where the bimolecular reaction is the limiting step. Next, we proceeded to the estimation of k_{cross} from the semilog plot of j versus E by the intercept at 0.29 V (vs SCE), which is in our experimental conditions the $E°$ value for the ferrocene labels. The value for k_{cross} obtained from this procedure was (2.2 ± 0.4) × 10^5 M^{-1} s^{-1}.

If we consider the critical role played by k_{cross} in the overall electron transfer process, two key questions come into light: How realistic is this k_{cross} value obtained from the ferrocene-labeled supramolecular bioconjugate? Does it have any actual physical meaning relevant to the electron transfer process? Moreover, previous work on electrochemical rectification via ferrocene-terminated self-assembled monolayers (as a surface-confined mediator) and ferrocyanide (as electron donor) reported a k_{cross} value corresponding to 1.1 × 10^8 M^{-1} s^{-1}.[17] This 3 orders of magnitude difference in k_{cross} for the same interacting species in different film architectures indicates molecular-level differences with strong implications on the electron exchange process.

To answer these questions we will consider an estimation of k_{cross} by the Marcus theory of electron transfer.[37] This framework provides the platform to evaluate and elucidate the different contributions convoluted in the value of the bimolecular electron transfer rate constant. In accordance with Marcus theory, k_{cross} is given by

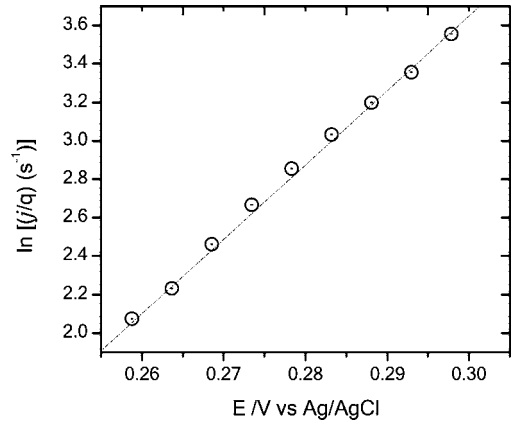

Figure 8. Semilog normalized current density (j/q) vs potential (E) plot for a Fc-SAv-modified Au electrode in a solution containing 120 μM $Fe(CN)_6^{4-}$ in 0.1 M PBS buffer. The slope of the linear representation is 38.68 V^{-1}.

$$k_{cross} \cong \sqrt{k_{11} k_{22} K_{12} f_{12}} \tag{9}$$

where k_{11} and k_{22} are the homogeneous electron self-exchange rate constants for the interacting redox species [$Fc^{0/+}$ and $Fe(CN)_6^{3-/4-}$]; K_{12} is the equilibrium constant of the reaction; and f_{12} is a known function of k_{11}, k_{22}, and K_{12} that is usually close to unity. To proceed with the estimation, we used recent data reporting the self-exchange rate constants for $Fc^{0/+}$ and $Fe(CN)_6^{3-/4-}$ in aqueous media. As derived from NMR line-broadening measurements, k_{11} is 3 × 10^6 M^{-1} s^{-1} for $Fc^{0/+}$[38] and k_{22} is 2 × 10^4 $M^{-1}s^{-1}$ for $Fe(CN)_6^{3-/4-}$.[39] To evaluate K_{12} from the Nernst equation, we need to consider that in our experimental scenario the formal potentials for the redox couples are 0.29 and 0.24 V (vs Ag/AgCl) for $Fc^{0/+}$ and $Fe(CN)_6^{3-/4-}$, respectively. This makes an equilibrium constant for the cross reaction of nearly 5. By introducing all these constant values in eq 9, we obtained an estimate for k_{cross} based on Marcus theory of ∼5.5 × 10^5 M^{-1} s^{-1}. Even by considering all the approximations introduced when comparing our experimentally determined k_{cross} with that predicted by Marcus theory, we can see a very close agreement between the two values. In addition, this agreement highlights two important points: (a) the AWC model is a simple and powerful tool for gaining insightful information on the electron transfer process, and (b) our experimental estimation of k_{cross} has a realistic value that is supported by the Marcus theory of electron transfer.

If we consider that our estimate of the rate constant of the cross reaction between $Fc^{0/+}$ and $Fe(CN)_6^{3-/4-}$ is valid and supported by a well-established and solid theory, then the remaining question is: Why do we observe a 3 orders of magnitude difference with other reported results obtained in a fairly similar environment with the same interacting species?

To address this question we need to refer back to the Marcus theory. The relevant parameters determining the value of k_{cross} are k_{11}, k_{22}, and K_{12}. Our rectifying interfacial architecture is based on ferrocene-labeled supramolecular bioconjugates interacting with $Fe(CN)_6^{4-}$ species in solution. Alleman et al.[17] worked with ferrocene-terminated SAMs rectifying the electrochemical current in the presence of $Fe(CN)_6^{4-}$. In both cases, due to the similarities in the experimental conditions, the values for k_{11} and k_{22} should not exhibit significant differences. Even if it is well-known that different solvent and ionic environments could affect the self-exchange rate constants, the reported data obtained under different experimental conditions indicate that (for each redox couple) the rate constants are of the same order

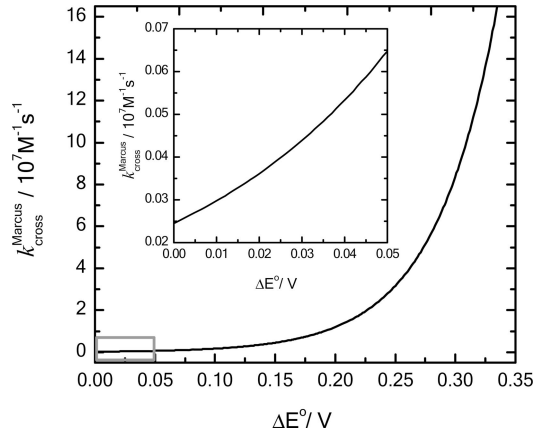

Figure 9. Theoretical representation of k_{cross} derived from the Marcus formalism, obtained by plotting eq 11 as a function of $\Delta E°$. The values of $k_{11}(Fc^{0/+}) = 2 \times 10^4\ M^{-1}\ s^{-1}$ and $k_{22}[Fe(CN)_6^{4-}] = 3 \times 10^6\ M^{-1}\ s^{-1}$ were taken from experimental data reported in the literature (see text for details). The value of $\Delta E°$ reflects the difference in formal potentials between donor and acceptor species interacting in the bimolecular electron transfer. (Inset) Enlarged view of the area delimited by the gray frame.

of magnitude.[40] This supports the idea that variations in the self-exchange rate constants are not a determinant factor explaining the major differences in k_{cross}.

On the other hand, when K_{12} values are compared, significant differences appear at first sight. K_{12} is evaluated from the Nernst equation by use of the formal potentials of donor and acceptor species under the given experimental conditions. Electrochemical rectification in ferrocene-terminated SAMs was carried out by Creager and co-workers[17] in the presence of $Fe(CN)_6^{4-}$ as electron donor and ferrocene as electron acceptor with the $E°$ values being +0.24 and +0.55 V (vs Ag/AgCl), respectively. For mediated electron transfer using redox-labeled supramolecular bioconjugates, the electron donor was also $Fe(CN)_6^{4-}$ with $E° = +0.25$ V (vs Ag/AgCl) but, in stark contrast, the formal potential for the surface-confined ferrocene labels was +0.29 V (vs Ag/AgCl). As a consequence, K_{12} for the $Fe(CN)_6^{4-}$/Fc-SAM system ($\Delta E° = 0.31$ V) is $\sim 1.7 \times 10^5$, while for the $Fe(CN)_6^{4-}$/Fc-SAv system ($\Delta E° = 0.04$ V) is only ~5. Differences of a few tenths of a volt can promote significant changes on the equilibrium constant when it is considering that

$$K_{12} = e^{nF\Delta E°/RT} \tag{10}$$

To further evidence the important role of differences in the formal potentials, let us describe k_{cross} derived from the Marcus formalism as a function of $\Delta E°$. We will make the simple assumption that k_{11} and k_{22} remain constant, even in different local environments. By introducing eq 10 into eq 9, we obtain

$$k_{cross}^{Marcus} = \sqrt{k_{11}k_{22}f_{12}e^{nF\Delta E°/RT}} \tag{11}$$

Figure 9 plots the expected dependence of k_{cross} on $\Delta E°$, using the Marcus expression (eq 9) as a framework to rationalize the differences observed between our results and those reported by Alleman et al.[17] The plot has been obtained by use of k_{11} and k_{22} data for ferrocene and ferrocyanide, respectively, taken from the literature.[38,39] Through this representation it can be observed that changes of ~0.3 V can promote variations of k_{cross} by orders of magnitude, thus reflecting the critical influence of the $E°$ shift on the value of the homogeneous rate constant.

In our experimental scenario, the reason to explain this striking difference in the formal potential of the acceptor lies in the fact that ferrocene groups are very sensitive to the characteristics of the surroundings. In a seminal work, Rowe and Creager[41] investigated the behavior of ferrocene moieties embedded in alkanethiolate SAMs of varying chain length. They found that the formal potential for ferrocene oxidation was shifted to more positive values as the ferrocene group was buried deeper into the hydrophobic environment. This potential shift reached nearly 0.3 V when the scenario changed from ferrocene groups totally exposed to the electrolyte solution to the same electroactive groups surrounded by a long-chain alkanethiol. The characteristics of the local environment at the molecular level play a key role in determining the relative stability of species involved in the redox couple. In the latter case, electrogeneration of ferricenium species in a hydrophobic poorly solvated environment is energetically more costly than in exposed hydrophilic surroundings. This is experimentally reflected in a positive shift of the formal potential. In the bioconjugated architecture, the redox labels are linked to the protein (diameter ~4−5 nm) by spacers 1−1.5 nm long, which can be interpreted as a scenario where the ferrocene groups are openly exposed to the surrounding electrolyte. Moreover, at pH 7.4 the protein is negatively charged,[42] further stabilizing the formation of ferricenium species. Hence, we ascribe the differences in formal potentials to changes in the local characteristics of the redox mediators, such as solvation, linker chain length, or electrostatic state of the medium (including the protein charge). It is worth mentioning that the negatively charged protein could also affect (diminish), by an electrostatic screening mechanism, the local concentration of $Fe(CN)_6^{4-}$ species near the ferrocene centers, resulting in a minor source of error in calculating the rate constants. More importantly, these results indicate that subtle changes at the molecular level in the local environment can promote drastic changes in electron transfer through the entire interfacial architecture.

Estimation of Standard Rate Constant for Electrochemical Reaction, k_o. The other key parameter necessary to achieve a full description of redox-mediated electron transfer is the standard rate constant for electrochemical oxidation/reduction of the surface-confined ferrocene groups (k_o). As previously discussed, increasing the donor concentration provokes the transition from case I to case II, where information about the magnitude of k_o is contained.

By analyzing the form of eq 8, we can see that a semilogarithmic j/q versus potential plot should describe a linear representation with a slope equivalent to $(1 - \alpha)$ times 38.96 V^{-1}, providing the value of k_o from the intercept at $E°$. A current−potential plot obtained from electrochemical experiments performed at high donor concentration (200 mM $Fe(CN)_6^{4-}$ in 0.1 M PBS) is depicted in Figure 10. As predicted by the AWC model, the plot shows a linear correspondence between ln (j/q) and potential, with a slope equal to 17.28 V^{-1}. This is the expected value for the case II regime, considering that the transfer (or symmetry) coefficients are typically close to 0.5.[43] To be more precise, the slope value would indicate that in our case α should be 0.55.

Once it was verified that we are in the proper regime, we proceeded to extract k_o from the intercept at $E°$. The corresponding k_o value was 24 s^{-1}. Once again we wonder how realistic this k_o value is and whether this value has any particular physical meaning. To further analyze this situation and for the sake of simplicity, we would better express k_o in terms of ln k_o. In our case, involving ferrocene-labeled supramolecular bioconjugates, ln k_o was 3.2 ± 0.2. A full description of the interfacial architecture, where the electron transfer from the

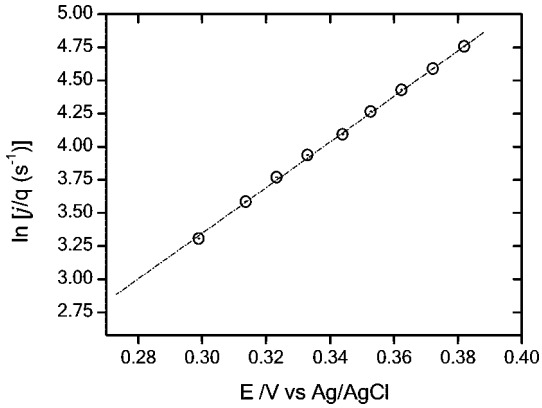

Figure 10. Semilog normalized current density (j/q) versus potential (E) plot for a Fc-SAv-modified Au electrode in a solution containing 200 mM $Fe(CN)_6^{4-}$ in 0.1 M in PBS buffer. The slope of the linear representation is 17.28 V^{-1}.

ferrocene labels to the gold electrode takes place, would involve three essential parts. The first one is the gold platform acting as an electron acceptor. The second one is the self-assembled monolayer containing the ligand sites where the electroactive protein is supramolecularly conjugated. The third one is the redox-labeled streptavidin containing the ferrocene moieties acting as donors in the electron transfer from protein to electrode. It is worth noticing that the biotinylated SAM is acting not only as a linker anchoring the redox-active centers but also as a "bridge" for electron transfer. Interfacial bridge-mediated electron transfer has been extensively studied in recent years,[44] especially the case describing electron transfer between Au electrodes and redox centers covalently attached to the electrode surface by different chain-length alkanethiols as molecular spacers.[45] It is well-known that in those cases electron transfer proceeds by tunneling across the hydrocarbon chain of the spacer where the chain length (donor−acceptor distance) play a key role on the overall process.[46] For a redox center attached to an electrode by a bridge of length d, which constitutes a mixed SAM composed of electrode−bridge−redox couple structures and diluent (nonelectroactive) alkanethiolates, the standard electron transfer rate constant is defined by

$$k_o(d) = k_o(0)e^{-\beta d} \tag{12}$$

or

$$\ln [k_o(d)] = \ln [k_o(0)] - \beta d \tag{13}$$

where β is the exponential decay exponent associated with the bridge and $k_o(0)$ includes the effect of the connection on the electronic coupling.[44] These parameters have been experimentally estimated and corroborated by different research groups.[44] From literature values, β is 1.01 ± 0.03 $Å^{-1}$ and ln $[k_o(0)]$ is 23.12 ± 0.47. An estimate of the thickness of our biotinylated platform obtained by surface plasmon resonance measurements indicated that our "spacer" is ∼2.0 nm.

Introducing this value into eq 13, we obtain a theoretical estimate of ln k_o of 2.9, which is in very good agreement with our experimental value. The similarities between the experimentally estimated k_o value and that obtained from eq 13 by use of a 2.0 nm long spacer strongly suggests that we are in the presence of bridge-mediated electron transfer between the redox labels and the gold electrode. The value of k_o could be mostly ascribed to the tunneling of electrons through the ligand-containing layer. Conversely, electron transfer through Fc-SAv probably occurs via a hopping mechanism, which is less affected by the donor−acceptor distance.[47] This assumption is supported by experimental results from different research groups.[48−50] These researchers demonstrated that electron transfer through peptide chains labeled with ferrocene centers is conducted by the hopping mechanism. This would indicate that, in our case, electron transfer between redox labels in the bioconjugated protein and the gold electrode is almost exclusively governed by tunneling across the biotinylated self-assembled monolayer.

Conclusions

In this work we have studied electron transfer between redox species in solution and Au electrodes mediated by ferrocene-labeled supramolecular bioconjugates. In order to gain understanding and rationalize the overall electron transfer process, we described the redox mediation in accordance with the model previously developed by Creager and co-workers[17] to study electrochemical rectification via self-assembled monolayers. In spite of its simplicity, the model describes quite nicely the experimental data obtained if electron transfer of $Fe(CN)_6^{4-}$ is electrocatalytically amplified/mediated by ferrocene labels linked to the protein layer. This approach enabled us to gain insight into the physicochemical and molecular aspects of the redox-mediated current, and to estimate the key parameters involved in the electron transfer process, k_{cross} and k_o. Our experimental results indicated that redox mediation can be described by two regimes. In one regime the limiting step in the overall process is the bimolecular reaction between oxidized mediator (electron acceptor) and electron donors in solution. This is experimentally observed when very low concentrations of the donor species are used. The other regime involves generation of the mediator species as the rate-limiting step in the redox mediation. This is evidenced when high donor concentrations, typically above 130 mM, are used.

Interestingly, the value of k_{cross} obtained in our experiments (2.2×10^5 M^{-1} s^{-1}) differs by 3 orders of magnitude compared to previously reported data for the same interacting species [$Fc^{0/+}$ and $Fe(CN)_6^{3-/4-}$]. In the latter case, redox mediators were diluted into a SAM. This significant change can be interpreted within the framework of the theory of Marcus, finding good agreement with the expected value. We ascribed these differences in k_{cross} to a marked $E°$ shift of the redox mediators in the supramolecular layer compared to the $E°$ value of the same redox mediators embedded in a SAM. This fact showed the critical role of the molecular environment in surface-confined systems in determining the magnitude of the bimolecular reaction constant, even for the same interacting species. Moreover, the obtained ln k_o value of 3.2 closely resembles previous experimental values describing electron transfer through SAMs of similar thickness to that used in our biotinylated platform. This observation strongly suggests that electron transfer between redox labels incorporated in the protein layer and the Au electrode is mostly governed by tunneling through the biotinylated SAM. We think that these results will have an impact on the molecular-level design of electrode surfaces to be used as biosensing platforms for electrocatalytic amplification.

Acknowledgment. O.A. is a CONICET member and acknowledges financial support from the Max Planck Society (Germany), the Alexander von Humboldt Stiftung (Germany), and the Centro Interdisciplinario de Nanociencia y Nanotecnología (CINN) (IP-PAE, ANPCyT−Argentina). M.Á. thanks Junta de Comunidades de Castilla la Mancha for a postdoctoral fellowship. B.Y. gratefully acknowledges financial support from Higher Education Commission (HEC) of Pakistan and Deutscher Akademischer Austauschdienst DAAD (Code A/04/30795).

References and Notes

(1) (a) Adams, D. M.; Brus, L.; Chidsey, C. E. D.; Creager, S. E.; Creutz, C.; Kagan, C. R.; Kamat, P. V.; Lieberman, M.; Lindsay, S.; Marcus, R. A.; Metzger, R. M.; Michel-Beyerle, M. E.; Miller, J. R.; Newton, M. D.; Rolison, D. R.; Sankey, O.; Schanze, K. S.; Yardley, J.; Zhu, X. *J.Phys. Chem. B* **2003**, *107*, 6668–6697. (b) Isied, S. S. In *Electron Transfer Reactions: Inorganic, Organometallic and Biological Applications*; American Chemical Society: Washington, DC, 1998. (c) Memming, R. In *Semiconductor Electrochemistry*; Wiley−VCH: Weinheim, Germany, 2001; Chapt. 6, pp 112−150. (d) Paddon-Row, M. N. In *Advances in Physical Organic Chemistry*, Vol. 38; Richard, J. P., Ed.; Elsevier Science: Oxford, U.K., 2003; pp 1−86. (e) Tributsch, H.; Pohlmann, L. *Science* **1995**, *279*, 1891.

(2) (a) Shipway, A. N.; Katz, E.; Willner, I. *ChemPhysChem* **2000**, *1*, 18–52. (b) *Biophysics of Electron Transfer and Molecular Bioelectronics*; Nicolini, C., Ed.; Springer: Heidelberg, Germany, 1999. (c) *Bioelectronics: From Theory to Applications*; Willner, I., Katz, E., Eds.; VCH−Wiley: Weinheim, Germany, 2005. (d) Balzani, V.; Credi, A.; Venturi, M. *Nanotoday* **2007**, *2*, 18–36.

(3) Keren, K.; Berman, R. S.; Buchstab, E.; Sivan, U.; Braun, E. *Science* **2003**, *302*, 1380.

(4) Braun, E.; Eichen, Y.; Sivan, U.; Ben-Yoseph, G. *Nature* **1998**, *391*, 775.

(5) (a) Kaifer, A. E.; Gómez-Kaifer, M. In *Supramolecular Electrochemistry*; VCH−Wiley: Weinheim, Germany, 2000. (b) Credi, A.; Ribera, B. F.; Venturi, M. *Electrochim. Acta* **2004**, *49*, 3865–3872.

(6) (a) *Organic Photochemistry and Photophysics*; Ramamurthy,V., Schanze, K. S., Eds.; CRC Press: Boca Raton, FL, 2006. (b) Balzani, V.; Scandola, F. In *Supramolecular Photochemistry*; Ellis Horwood: Chichester, U.K., 1991. (c) Balzani, V.; Credi, A.; Venturi, M. In *Molecular Devices and Machines: A Journey into the Nanoworld*; VCH−Wiley; Weinheim, Germany, 2003.

(7) Ferrer, B.; Rogez, G.; Credi, A.; Ballardini, R.; Gandolfi, M. T.; Balzani, V.; Liu, Y.; Tseng, H. R.; Stoddart, J. F. *Proc. Natl. Acad. Sci. U.S.A.* **2006**, *103*, 18411–18416.

(8) Collier, C. P.; Jeppesen, J. O.; Luo, Y.; Perkins, J.; Wong, E. W.; Heath, J. R.; Stoddart, J. F. *J. Am. Chem. Soc.* **2001**, *123*, 12632–12641.

(9) (a) Lindsay, S. M.; Ratner, M. A. *Adv. Mater.* **2007**, *19*, 23–31. (b) Joachim, C.; Ratner, M. A. *Proc. Natl. Acad. Sci. U.S.A.* **2005**, *102*, 8801–8808. (c) Nitzan, A.; Ratner, M. A. *Science* **2003**, *300*, 1384–1389. (d) James, D. K.; Tour, J. M. In *Nanoscale Assembly: Chemical Techniques*; Huck, W. T. S., Ed.; Springer: Heidelberg, Germany, 2005; Chapt. 5, pp 79−98.

(10) (a) Metzger, R. M. *Chem. Rec.* **2004**, *4*, 291–304. (b) Metzger, R. M. *Chem. Rev.* **2003**, *103*, 3803–3834.

(11) (a) Chabinyc, M. L.; Chen, X.; Holmlin, R. E.; Jacobs, H.; Skulason, H.; Frisbie, C. D.; Mujica, V.; Ratner, M. A.; Rampi, M. A.; Whitesides, G. M. *J. Am. Chem. Soc.* **2002**, *124*, 11730–11736. (b) Metzger, R. M.; Baldwin, J. W.; Shumate, W. J.; Peterson, I. R.; Mani, P.; Mankey, G. J.; Morris, T.; Szulczewski, G.; Bosi, S.; Prato, M.; Comito, A.; Rubin, Y. *J. Phys. Chem. B* **2003**, *107*, 1021–1027. (c) Baldwin, J. W.; Amaresh, R. R.; Peterson, I. R.; Shumate, W. J.; Cava, M. P.; Amiri, M. A.; Hamilton, R.; Ashwell, G. J.; Metzger, R. M. *J. Phys. Chem. B* **2002**, *106*, 12158–12164. (d) Honciuc, A.; Jaiswal, A.; Gong, A.; Ashworth, K.; Spangler, C. W.; Peterson, I. R.; Dalton, L. R.; Metzger, R. M. *J. Phys. Chem. B* **2005**, *109*, 857–871. (e) Metzger, R. M.; Xu, T.; Peterson, I. R. *J. Phys. Chem. B* **2001**, *105*, 7280–7290. (f) Ashwell, G. J.; Mohib, A. *J. Am. Chem. Soc.* **2005**, *127*, 16238–16244. (g) Ashwell, G. J.; Tyrrell, W. D.; Whittam, A. J. *J. Am. Chem. Soc.* **2004**, *126*, 7102–7110. (h) Lenfant, S.; Guerin, D.; Tran Van, F.; Chevrot, C.; Palacin, S.; Bourgoin, J. P.; Bouloussa, O.; Rondelez, F.; Vuillaume, D. *J. Phys. Chem. B* **2006**, *110*, 13947–13958. (i) Cayre, O. J.; Chang, S. T.; Velev, O. D. *J. Am. Chem. Soc.* **2007**, *129*, 10801–10806.

(12) (a) Murray, R. W. *Philos. Trans. R. Soc. London, Ser. A* **1981**, *302*, 253–265. (b) Murray, R. W. In *Electroanalytical Chemistry*; Bard, A. J., Ed.; Marcel Dekker: New York, 1984; Vol. 13, pp 191−368. (c) Chidsey, C. E. D.; Murray, R. W. *Science* **1986**, *231*, 25.

(13) (a) Abruña, H. D. In *Electroresponsive Molecular and Polymeric Systems*, Vol. 1; Skotheim, T. A., Ed.; Marcel Dekker: New York, 1988; Chapt. 3, pp 97−171. (b) Abe, T.; Kaneko, M. *Prog. Polym. Sci.* **2003**, *28*, 1441–1488.

(14) (a) Savéant, J. M. *J. Electroanal. Chem.* **1988**, *242*, 1–21. (b) Savéant, J. M. *J. Electroanal. Chem.* **1986**, *201*, 211–213. (c) Majda, M. In *Molecular Design of Electrode Surfaces*; Murray, R. W., Ed.; Wiley: New York, 1992; Chapt. 4, p 159. (d) Lyons, M. E. G. In *Electroactive Polymer Electrochemistry Part 1: Fundamentals*; Lyons, M. E. G., Ed.; Plenum Press: New York, 1994; Chapt. 1, p M1.

(15) (a) Berchams, S.; Usha, S.; Ramalechume, C.; Yegnaraman, J. *Solid. State. Electrochem.* **2005**, *9*, 595. (b) Maksymiuk, K.; Doblhofer, K. *Electrochim. Acta* **1994**, *39*, 217–227. (c) Doblhofer, K.; Armstrong, M. D. *Electrochim. Acta* **1988**, *33*, 453–460.

(16) (a) Xie, Y.; Anson, F. C. *J. Electroanal. Chem.* **1995**, *384*, 145–153. (b) Amarasinghe, S.; Chen, T.; Moberg, P.; Paul, H. J.; Tinoco, F.; Zook, L. A.; Leddy, J. *Anal. Chim. Acta* **1995**, *307*, 227–244. (c) Andrieux, C. P.; Dumas-Bouchiat, J. M.; Savéant, J. M. *J. Electroanal. Chem.* **1982**, *131*, 1–35.

(17) Alleman, K. S.; Weber, K.; Creager, S. E. *J. Phys. Chem.* **1996**, *100*, 17050–17058.

(18) (a) Niemeyer, C. M. In *Nanobiotechnology: Concepts, Applications and Perspectives*; Niemeyer, C. M., Mirkin, C. A., Eds.; VCH−Wiley: Weinheim, Germany, 2004; Chapt. 15, p 227. (b) Katz, E.; Willner, I. *Angew. Chem., Int. Ed.* **2004**, *43*, 6042–6108. (c) Deans, R.; Cuello, A. O.; Galow, T. H.; Ober, M.; Rotello, V. M. *J. Chem. Soc., Perkin Trans.* **2000**, *2*, 1309–1313.

(19) (a) Long, D. P.; Lazorcik, J. L.; Mantooth, B. A.; Moore, M. H.; Ratner, M. A.; Troisi, A.; Yao, Y.; Ciszek, J. W.; Tour, J. M.; Shashidhar, R. *Nat. Mater.* **2006**, *5*, 901–908. (b) Yaliraki, S. N.; Kemp, M.; Ratner, M. A. *J. Am. Chem. Soc.* **1999**, *121*, 3428–3434. (c) Yaliraki, S. N.; Ratner, M. A. *J. Chem. Phys.* **1998**, *109*, 5036–5043. (d) Seminario, J. N.; Zacarias, A. C.; Tour, J. M. *J. Am. Chem. Soc.* **1999**, *121*, 411–416.

(20) Shoham, B.; Migron, Y.; Riklin, A.; Willner, I.; Tartakovsky, B. *Biosens. Bioelectron.* **1995**, *10*, 341–352.

(21) (a) Padeste, C.; Grubelnik, A.; Tiefenauer, L. *Biosens. Bioelectron.* **2003**, *19*, 239. (b) Padeste, C.; Steiger, B.; Grubelnik, A.; Tiefenauer, L. *Biosens. Bioelectron.* **2004**, *20*, 545. (c) Steiger, B.; Padeste, C.; Grubelnik, A.; Tiefenauer, L. *Electrochim. Acta* **2003**, *48*, 761.

(22) Knoll, W. *Annu. Rev. Phys. Chem.* **1998**, *49*, 569.

(23) (a) Stenberg, E.; Persson, B.; Roos, H.; Urbaniczky, C. *J. Colloid Interface Sci.* **1991**, *143*, 513–526. (b) Yu, F. Ph.D. Thesis, Johannes Gutenberg-Universität, Mainz, Germany, 2004; http://www.mpip-mainz.mpg.de/knoll/publications/thesis/yu2004.pdf.

(24) (a) Spinke, J.; Liley, M.; Schmitt, F.-J.; Guder, H.-J.; Angermaier, L.; Knoll, W. *J. Chem. Phys.* **1993**, *99*, 7012–7019. (b) Pérez-Luna, V. H.; O'Brien, M. J.; Opperman, K. A.; Hampton, P. D.; López, G. P.; Klumb, L. A.; Stayton, P. S. *J. Am. Chem. Soc.* **1999**, *121*, 6469–6478.

(25) Smith, C. L.; Milea, J. S.; Nguyen, G. H. *Top. Curr. Chem.* **2006**, *261*, 63–90.

(26) Azzaroni, O.; Mir, M.; Knoll, W. *J. Phys. Chem. B* **2007**, *111*, 13499–13503.

(27) Nelson, K. E.; Gamble, L.; Jung, L. S.; Boeckl, M. S.; Naeemi, E.; Golledge, S. L.; Sasaki, T.; Castner, D. G.; Campbell, C. T.; Stayton, P. S. *Langmuir* **2001**, *17*, 2807–2816.

(28) Ihalainen, P.; Peltonen, J. *Sens. Actuators, B* **2004**, *102*, 207–218.

(29) (a) Coen, M. C.; Lehmann, R.; Fröning, P.; Bielmann, M.; Calli, C.; Schlabach, L. *J. Colloid Interface Sci.* **2001**, *233*, 180–189. (b) Cooper, J. M.; Shen, J.; Young, F. M.; Connolly, P.; Baker, J. R.; Moores, G. *J. Mater. Sci.* **1994**, *5*, 106–110.

(30) Wilder, K.; Quate, C. F.; Singh, B.; Alvis, R.; Arnold, W. H. *J. Vac. Sci. Technol., B* **1996**, *14*, 4004–4008.

(31) (a) Hansma, H. G.; Weisenhorn, A. L.; Gould, S. A. C.; Sinsheimer, R. L.; Gaub, H. E.; Stucky, G. D.; Zaremba, C. M.; Hansma, P. K. *J. Vac. Sci. Technol., B* **1991**, *9*, 1282. (b) Wisenhorn, A. L.; Egger, M.; Ohnesorge, F.; Gould, S. A. C.; Heyn, S.-P.; Hansma, H. G.; Sinsheimer, R. L.; Gaub, H. E.; Hansma, P. K. *Langmuir* **1991**, *7*, 8. (c) Bustamante, C.; Vesenka, J.; Tang, C. L.; Rees, W.; Guthold, M.; Keller, R. *Biochemistry* **1992**, *31*, 22. (d) Kossek, S.; Padeste, C.; Tiefenauer, L. X.; Siegenthaler, H. *Biosens. Bioelectron.* **1998**, *13*, 31–43.

(32) Finklea, H. O. In *Electroanalytical Chemistry*; Bard, A. J., Rubinstein, I., Eds.; Marcel Dekker: New York, 1996; Vol. 19, pp 109−335.

(33) Finklea, H. O.; Avery, S.; Lynch, M.; Furtsch, T. *Langmuir* **1987**, *3*, 409–413.

(34) Oh, S. K.; Baker, L. A.; Crooks, R. M. *Langmuir* **2002**, *18*, 6981.

(35) (a) Feldberg. S. W.; Newton, M. D.; Smalley, J. F. In *Electroanalytical Chemistry*, Vol 22; Bard, A. J., Rubinstein, I., Eds.; Marcel Dekker, New York, 2004; pp 101−180. (b) Schmickler, W. In *Interfacial Electrochemistry*; Oxford University Press: New York, 1996; Chapt. 5, p 62.

(36) Bard, A. J.; Faulkner, L. R. *Electrochemical Methods: Principles and Applications*; Wiley: New York, 2000.

(37) (a) Marcus, R. A. *Angew. Chem., Int. Ed.* **1993**, *32*, 1111–1121. (b) Marcus, R. A.; Sutin, N. *Biochim. Biophys. Acta* **1985**, *811*, 265–322. (c) Marcus, R. A. *Annu. Rev. Phys. Chem.* **1964**, *15*, 155–196.

(38) Yuan, L.; Macartney, D. H. *J. Phys. Chem. B* **2007**, *111*, 6949–6954.

(39) Royea, W. J.; Hamann, T. W.; Brunschwig, B. S.; Lewis, N. S. *J. Phys. Chem. B.* **2006**, *110*, 19433–19442.

(40) (a) Kirchner, K.; Dang, S. Q.; Stebler, M.; Dodgen, H. W.; Wherland, S.; Hunt, J. P. *Inorg. Chem.* **1989**, *28*, 3604–3606. (b) Shporer, M.; Ron, G.; Loewenstein, A.; Navon, G. *Inorg. Chem.* **1965**, *4*, 361–364. (c) Kurland, R. J.; Winkler, M. E. *J. Biochem. Biophys. Methods* **1981**, *4*, 215–225. (d) Takagi, H.; Swaddle, T. W. *Inorg. Chem.* **1992**, *31*, 4669–4673. (e) McManis, G. E.; Nielson, R. M.; Gochev, A.; Weaver, M. J. *J. Am.*

Chem. Soc. **1989**, *111*, 5533–5541. (f) Nielson, R. M.; McManis, G. E.; Safford, L. K.; Weaver, M. J. *J. Phys. Chem.* **1989**, *93*, 2152–2157.

(41) Rowe, G. K.; Creager, S. E. *Langmuir* **1991**, *7*, 2307–2312.

(42) (a) Leckband, D. E.; Schmitt, F.-J.; Israelachvili, J. N.; Knoll, W. *Biochemistry* **1994**, *33*, 4611–4624. (b) Sivasankar, S.; Subramaniam, S.; Leckband, D. *Proc. Natl. Acad. Sci. U.S.A.* **1998**, *95*, 12961–12966.

(43) Schmickler, W. *Interfacial Electrochemistry*; Oxford University Press: New York, 1996; Chapt. 9, p 123.

(44) (a) Newton, M. D.; Smalley, J. F. *Phys. Chem. Chem. Phys.* **2007**, *9*, 555–572.

(45) (a) Smalley, J. F.; Newton, M. D.; Feldberg, S. W. *J. Electroanal. Chem.* **2006**, *589*, 1–6. (b) Miller, C. J. In *Physical Electrochemistry: Principles, Methods and Applications*; Rubinstein, I., Ed.; Marcel Dekker: New York, 1995; Chapt.2, pp 27−92. (c) Finklea, H. O.; Hanshew, D. D. *J. Am. Chem. Soc.* **1992**, *114*, 3133–3181. (d) Smalley, J. F.; Finklea, H. O.; Chidsey, C. E. D.; Linford, M. R.; Creager, S. E.; Ferraris, J. P.; Chalfant, K.; Zawodzinsk, T.; Feldberg, S. W.; Newton, M. D. *J. Am. Chem. Soc.* **2003**, *125*, 2004–2013. (e) Smalley, J. F.; Sachs, S. B.; Chidsey, C. E. D.; Dudek, S. P.; Sikes, H. D.; Creager, S. E.; Yu, C. J.; Feldberg, S. W.; Newton, M. D. *J. Am. Chem. Soc.* **2004**, *126*, 14620–14630. (f) Slowinski, K.; Chamberlain, R. V.; Miller, C. J.; Majda, M. *J. Am. Chem. Soc.* **1997**, *199*, 11910–11919. (g) Sumner, J. J.; Creager, S. E. *J. Phys. Chem. B* **2001**, *105*, 8739–8745. (h) Terretazz, S.; Becka, A. M.; Traub, M. J.; Fettinger, J. C.; Miller, C. J. *J. Phys. Chem.* **1995**, *99*, 11216–11224. (i) Sikes, H. D.; Smalley, J. F.; Dudek, S. P.; Cook, A. R.; Newton, M. D.; Chidsey, C. E. D.; Feldberg, S. W. *Science* **2001**, *291*, 1519–1523.

(46) (a) Smalley, J. F.; Feldberg, S. W.; Chidsey, C. E. D.; Linford, M. R.; Newton, M. D.; Li, Y.-P. *J. Phys. Chem.* **1995**, *99*, 13141–13149. (b) Smalley, J. F. *J. Phys. Chem. B* **2007**, *111*, 6798–6806. (c) Newton, M. D.; Sutin, N. *Annu. Rev. Phys. Chem.* **1984**, *35*, 437–80.

(47) (a) Malak, R. A.; Gao, Z.; Wishart, J. F.; Isied, S. S. *J. Am. Chem. Soc.* **2004**, *126*, 13888–13889. (b) Berlin, Y. A.; Ratner, M. A. *Radiat. Phys. Chem.* **2005**, *74*, 124–131.

(48) Sek, S.; Sepiol, A.; Tolak, A.; Misicka, A.; Bilewicz, R. *J. Phys. Chem. B* **2004**, *108*, 8102–8105.

(49) (a) Morita, T.; Kimura, S. *J. Am. Chem. Soc.* **2003**, *125*, 8732–8733. (b) Kitagawa, K.; Morita, T.; Kimura, S. *Langmuir* **2005**, *21*, 10624–10631. (c) Kitagawa, K.; Morita, T.; Kimura, S. *J. Phys. Chem. B* **2005**, *109*, 13906–13911. (d) Watanabe, J.; Morita, T.; Kimura, S. *J. Phys. Chem. B* **2005**, *109*, 14416–14425.

(50) (a) Long, Y.-T.; Abu-Irhayem, E.; Kraatz, H.-B. *Chem.—Eur. J.* **2005**, *11*, 5186–5194. (b) Dey, S. K.; Mandal, H. S.; Long, Y.-T.; Chowdhury, S.; Sutherland, T. C.; Kraatz, H.-B. *Langmuir* **2007**, *23*, 6475–6477.

JP804938M